

Optical Engineering

OpticalEngineering.SPIEDigitalLibrary.org

Automated calibration of an optomechanical derotator using 6-axes parallel kinematics and industrial image processing algorithms

Benjamin Rohloff
Christian Pape
Eduard Reithmeier

Automated calibration of an optomechanical derotator using 6-axes parallel kinematics and industrial image processing algorithms

Benjamin Rohloff,* Christian Pape, and Eduard Reithmeier

Leibniz University Hannover, Faculty of Mechanical Engineering, Institute of Measurement and Automatic Control, Nienburger Strasse 17, 30167 Hannover, Germany

Abstract. A concept for an optomechanical derotator is presented. The derotator allows optical measurements of rotating objects during operation. To guarantee a stationary optical image, the optical axis of the derotator needs to be coaxially aligned to the rotational axis of the measured object. The correlation between the movement of the optical image and a miscalibration is explained by a mathematical model. The movement of the optical image is tracked with a high-speed camera. Approximating the tracked path as a Limacon of Pascal, a parameter corresponding to the magnitude of the miscalibration is identified. This parameter is minimized by modifying the position and the orientation of the derotator with a hexapod. The limitations of this procedure are analyzed and further approaches are discussed. © The Authors. Published by SPIE under a Creative Commons Attribution 3.0 Unported License. Distribution or reproduction of this work in whole or in part requires full attribution of the original publication, including its DOI. [DOI: [10.1117/1.OE.53.10.104101](https://doi.org/10.1117/1.OE.53.10.104101)]

Keywords: derotator; calibration; rotating objects; optical measurement systems.

Paper 140935V received Jun. 11, 2014; revised manuscript received Aug. 26, 2014; accepted for publication Sep. 8, 2014; published online Oct. 6, 2014.

1 Introduction

To investigate rotating objects during operation, noncontact measurement methods are increasingly preferred because they do not affect the physical properties of the measured objects. Industrial image processing, infrared measurement technology, as well as the laser Doppler vibrometry are the examples for such noncontact measurement methods. All coordinate systems of those methods are usually located in the stationary laboratory coordinate system. Using an optomechanical derotator, a transformation into the rotating coordinate system of the measured object can be achieved. Reference 1, for example, investigates the slip in rolling bearings using a derotator based on a rotating dove prism. The investigations are supplemented by measurements with a laser Doppler vibrometer at a cut-off wheel. This approach is also taken by Refs. 2 and 3 and used for the identification of the vibrational modes of a saw blade. Using a derotator with a dove prism, typical artifacts occur resulting from the use of lenses. Reference 4 discusses these problems in detail and presents a new concept for a derotator as explained in the following section. Using such a derotator, Ref. 5 makes vibration tests on a model of a blisk, identifying the effects of phenomena such as centrifugal stiffening of the blade.

2 Experimental Equipment

The effect of derotation occurs with a rotating mirror assembly, which consists of a metallic reflector prism and an eccentrically positioned reflector, as shown in Fig. 1. For an accurate derotation, it is necessary that the reflectors rotate with half of the speed of the measured object. To

achieve this condition, the reflector assembly is mounted in a specially built, high-performance hollow shaft motor. The motor is characterized by its high dynamic behavior and a maximum speed of 12,000 rpm. Thus, objects can rotate up to 24,000 rpm.

Figure 2 shows the whole experimental setup. All components are monitored and controlled by a real-time system. Some of the control loops are outsourced to external controllers. Our current work aims at identifying and controlling the drivetrain components of the subsystem consisting of the derotator and controller II. During speed changes, the influence of nonlinear effects such as friction cannot be neglected. Linear control concepts do not provide the necessary speed coupling.

Another basic requirement for an accurate derotation is the position of the rotational axis of the measured object related to the position of the optical axis of the reflector system. If the two axes are not coaxial, then precise measuring is not possible due to a residual movement of the optical image. Hereinafter, this state is referred to as an imperfect calibration. To reduce the residual movement, the derotator is installed on a 6-axes parallel kinematics (Newport HXP1000, Irvine, California, minimum incremental motion translational $\leq 0.3 \mu\text{m}$, rotational $\leq 1 \mu\text{rad}$), enabling an accurate positioning process.

3 Mathematical Model of the Optical Image

This section aims to provide a model of the optical image. Using this model, a calibration strategy can be developed in the next section. The following considerations are based on the work of Ref. 6, investigating a derotator of a different design. Considering an arbitrary point on the measured object, the movement of this point in the image plane can be described by the following equation:

*Address all correspondence to: Benjamin Rohloff, E-mail: benjamin.rohloff@imr.uni-hannover.de

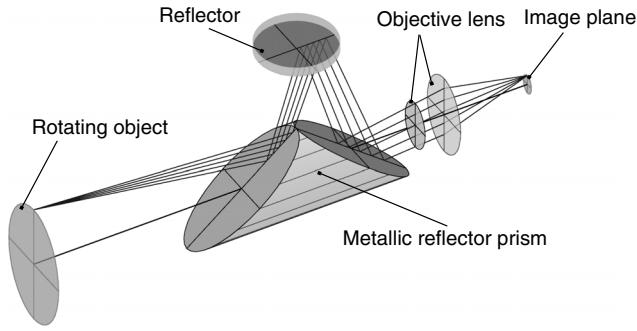


Fig. 1 Rotating reflector assembly as a core element of the derotator.

$$\begin{aligned}
 \begin{bmatrix} x(t) \\ y(t) \end{bmatrix} &= \underbrace{\begin{bmatrix} r \cos(\varphi_0) \\ -r \sin(\varphi_0) \end{bmatrix}}_I \\
 &+ \underbrace{\begin{bmatrix} \cos[2\delta(t)] & \sin[2\delta(t)] \\ \sin[2\delta(t)] & -\cos[2\delta(t)] \end{bmatrix}}_{II} \cdot \begin{pmatrix} -d_x \\ -d_y \end{pmatrix} \\
 &+ \underbrace{\begin{bmatrix} d_f \sin[\delta(t)] \\ -d_f \cos[\delta(t)] \end{bmatrix}}_{III}. \tag{1}
 \end{aligned}$$

A detailed derivation of this equation can be found in Refs. 7 and 8 consisting of simple coordinate transformations, the total beam path modeled with methods of the analytic geometry, and a simplified camera model with a so-called thin lens. If the optical axis of the derotator is coaxially aligned to the rotational axis of the measured object, then the terms II and III are omitted. The optical image is dependent on the distance to the object center r and the phase shift between the object and the derotator. If the two axes are not coaxially aligned to each other, then term II describes a circular movement in the image plane. Depending on the rotational angle $\delta(t)$, this motion is carried out by all

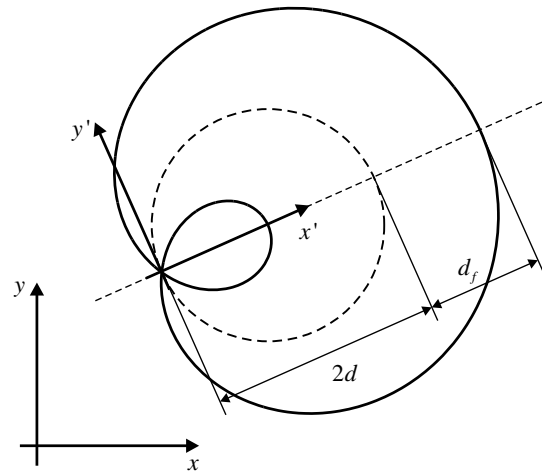


Fig. 3 Trajectory of all points on the measured object in the image plane.

points on the measured object at the same time. The intensity is determined by the offset d_x, d_y between the rotational axis of the object and the optical axis of the derotator. Considering small angles, Ref. 8 has shown that the tiltings can be expressed by parallel shifts. The associated problems are discussed below. In the case of coaxially aligned axes, an error in the reflector adjustment is modeled by term III. The error is given by the deviation d_f from the optimum distance between the metallic reflector prism and the excentrically mounted reflector. Additionally, this case results in a circular movement of the image depending on the rotational angle. The real system has an error in the reflector adjustment (term III) and an imperfect calibration (term II). For the following step, some trigonometric transformations and the substitution $(\delta - \gamma) = [\varphi + (\pi/2)]$ are necessary. Assuming a parallel shift

$$\begin{pmatrix} d_x \\ d_y \end{pmatrix} = \begin{pmatrix} d \cos \gamma \\ d \sin \gamma \end{pmatrix}, \tag{2}$$

with an absolute value d and an angle γ , it is possible to transform Eq. (1) to

$$x' = 2d \cos^2 \varphi + d_f \cos \varphi, \tag{3}$$

and

$$y' = 2d \cos \varphi \sin \varphi + d_f \sin \varphi. \tag{4}$$

Equations (3) and (4) describe a special case of a general conchoid called the Limaçon of Pascal, as shown in Fig. 3.

The following section explains the identification of the parameter $2d$, which is a measure of the miscalibration.

4 Development of a Calibration Procedure

Reducing the work of image processing, a simple to be measured object, as shown in Fig. 4, is analyzed. Problems occurring due to an incorrect rotational speed coupling can be neglected if the marker on the rotational axis of the measured object is considered. By using simple industrial image

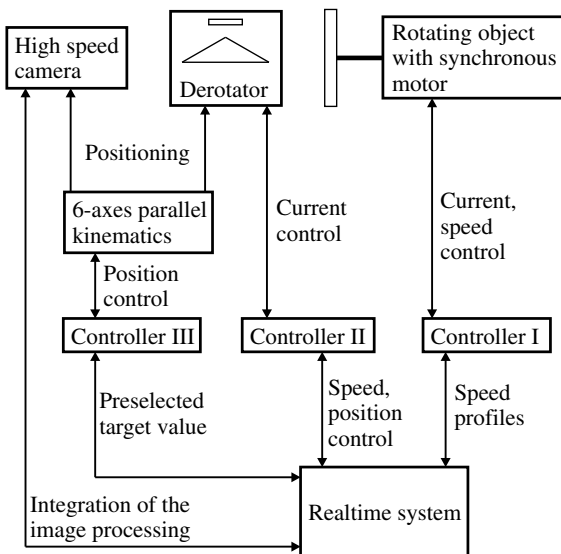


Fig. 2 Complete experimental setup.

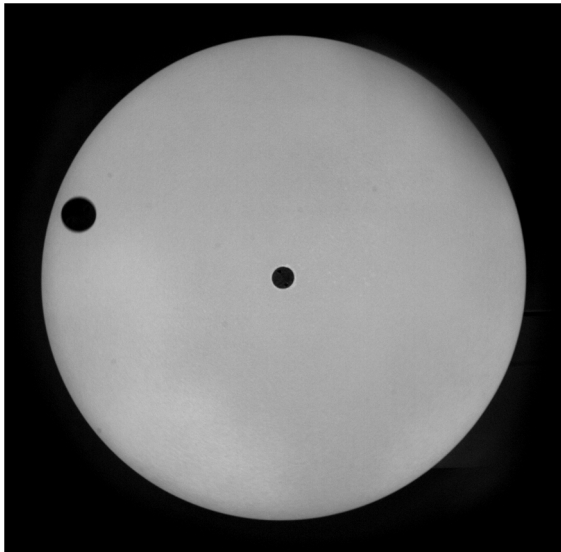


Fig. 4 Simple to be measured object, aluminum, diameter 220 mm, beamless white, two black markers of different sizes.

processing algorithms, like binary segmentation, the position of the marker on the rotational axis can be detected (Ref. 9).

To analyze the movement of the marker, 360 pictures are taken with the high-speed camera (Mikrotron MC1362, Unterschleissheim, Germany, resolution 1280×1024 pixels, pixel size $14 \mu\text{m}$, speed 506 frames/s at full resolution using a Tamron lens 1: 3.975 mm $\varnothing 25.5$) during one rotation of the derotator, the center of the marker is calculated, and the results are exemplarily shown in Fig. 5.

To identify the extent of miscalibration, the measured data need to be approximated as a Limacon of Pascal. Prior to the resulting optimization problem, the point of origin of the curve is determined and the measured data are sorted. Thereby, the measured data are transformed into the coordinate system x', y' (Fig. 3). For the subsequent identification of the parameters, the particle swarm algorithm is used

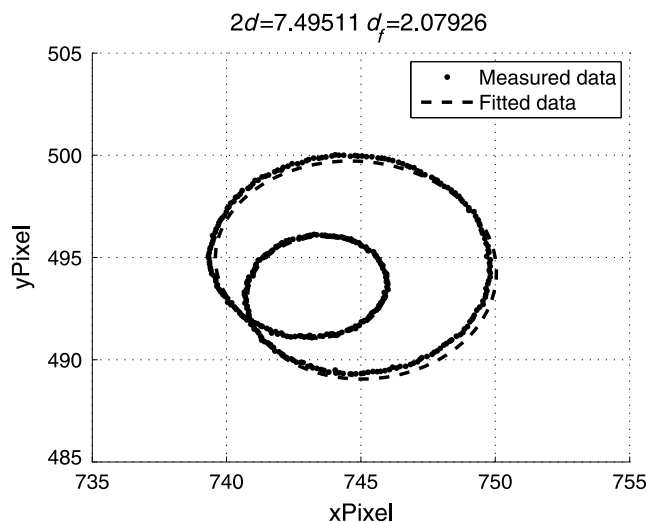


Fig. 5 Example of an image movement resulting from a miscalibration and the approximation of the Limacon of Pascal.

because it has been proven in various approximation problems of measurement data to be a robust and accurate method. Contrary to the recommendation in Ref. 10, the direction of movement of an individual of the swarm is determined by the experience of the swarm with increasing iterations. Using a dashed line, the result of such an identification is illustrated in Fig. 5. The extent of miscalibration is estimated at $2d = 7.5$ pixel, and the error of the reflector adjustment amounts to $d_f = 2.1$ pixel.

By adjusting the position of the derotator, it is possible to reduce the value of $2d$. To solve this optimization problem, the simplex method developed by Nelder and Mead is chosen.¹¹ This method was used because the solution process corresponds to a movement through the generated solution space. This movement is associated with real motions of the parallel kinematics. A single simplex consists of four dimensions $p = (x, y, \alpha, \beta)$. Motions of the parallel kinematics in the direction z and around the optical axis of the derotator (angle γ) are excluded, because they do not result in the calculated objective value. During the optimization, the hexapod automatically moves to different positions, 360 pictures are taken, and the extent of the miscalibration is calculated using the particle swarm algorithm. The decision as to which direction is chosen in the solution space is made with the help of the method of Nelder and Mead. In the following section, a calibration procedure is presented.

5 Implementation of the Calibration Procedure

For the verification of the calibration procedure, a measurement situation is assumed. The exact position of the measured object in the laboratory coordinate system is unknown. The derotator mounted on the parallel kinematics is roughly positioned in front of the measured object, wherein the hexapod is located at the origin of its coordinate system $p = (0 \text{ mm}, 0 \text{ mm}, 0 \text{ deg}, 0 \text{ deg})$. The movement of the optical image in this kind of situation can be seen in Fig. 7(a). At this time, the parameter is $2d = 211.5$ pixels meaning that the miscalibration is very large. Activating the automatic calibration procedure, an initialization takes place, because for solving the four-dimensional optimization problem the Nelder–Mead algorithm needs five starting positions. The entire iteration process is shown in Fig. 6.

After a couple of iterations, the parameter $2d = 37.1$ pixel is significantly reduced at iteration point 2, as shown in Fig. 7(b). Iteration point 3 [Fig. 7(c)] illustrates the typical motion of the image, which has already been mentioned in the model. The amount of the internal motion resulting from the miscalibration can be further reduced ($2d = 7.5$ pixel).

Reaching iteration point 4 [Fig. 7(d)], a new problem occurs. The approximation of the measured data as a Limacon of Pascal is no longer suitable. The amount of the miscalibration d_x, d_y in term II of Eq. (1) is reduced to such a level that the misalignment dominates and an elliptical motion ensues. Regarding the density of the dots in the upper range of the measured data ($x\text{Pixel} = 742 - 746, y\text{Pixel} = 495 - 496$), a residual internal image motion seems to be still present, but cannot be identified with this approach. The particle swarm algorithm needs to be extended by the possibility of approximating an ellipse. Reinitializing the calibration procedure, the objective values rise in Fig. 6 at iteration 25. On one hand, the increasing objective values depend on the reinitialization, and on the

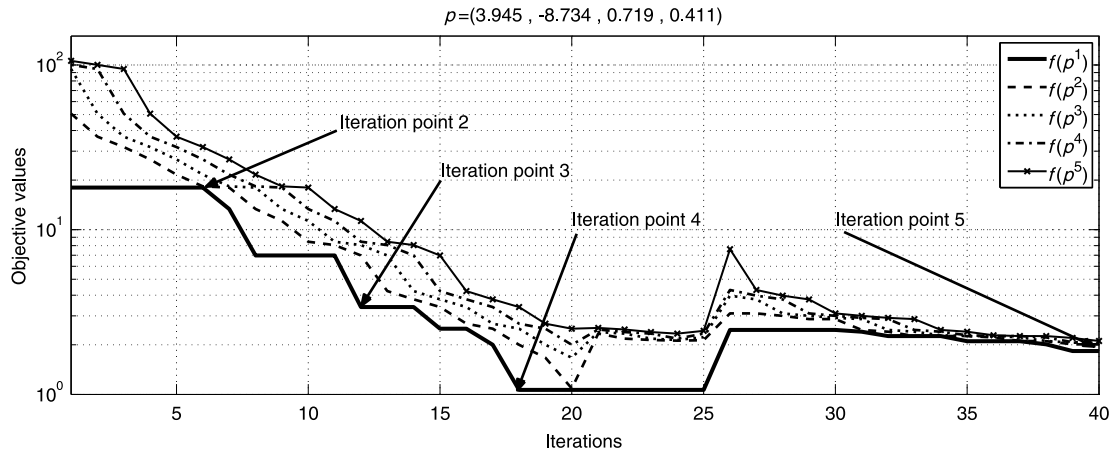


Fig. 6 Progress of the objective values $f(p)$. The iteration points 2 to 5 are discussed in detail in the text.

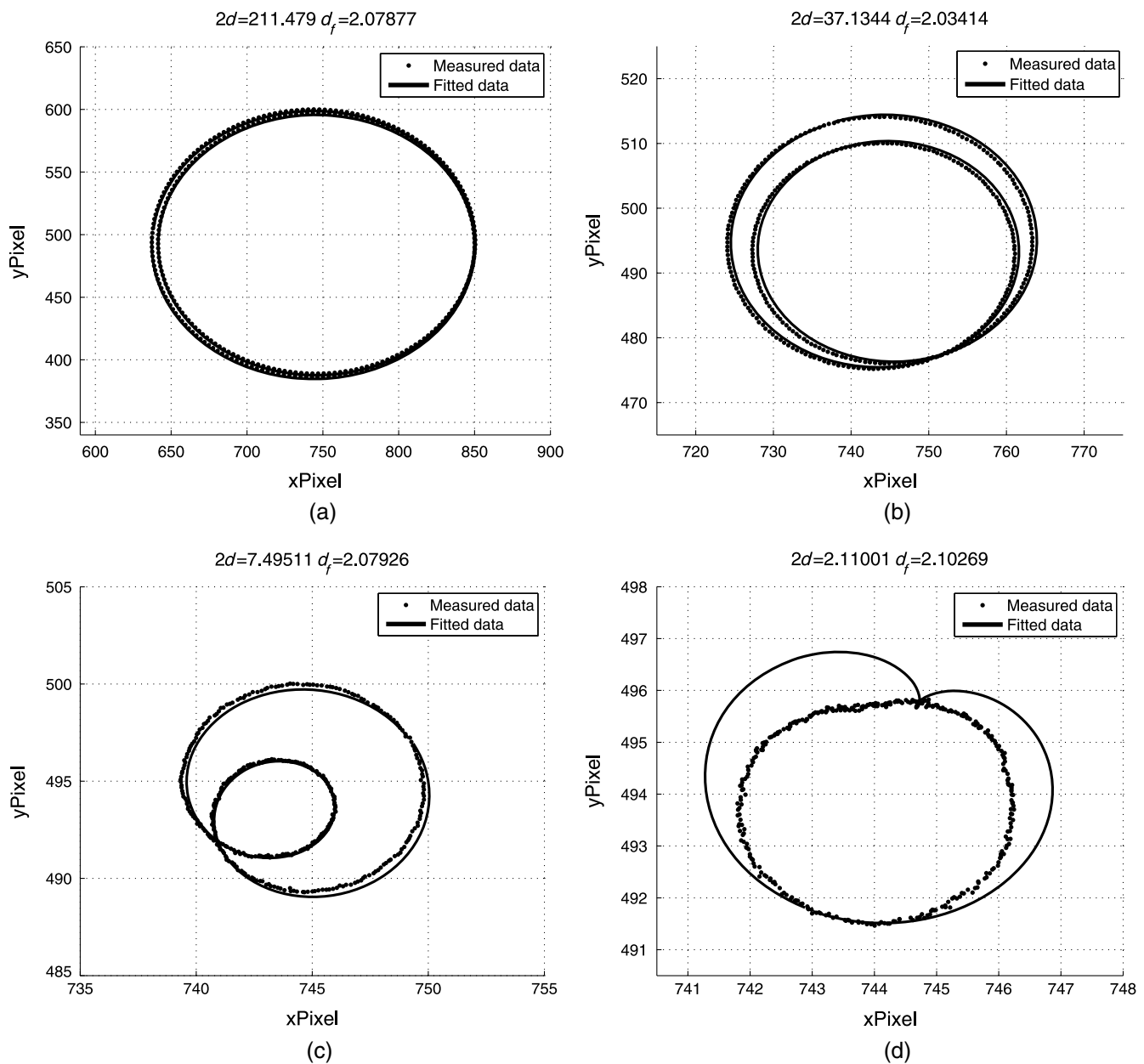


Fig. 7 Movement of the optical image: (a) Zero position of the hexapod. (b–d) Iteration points 2 to 4.

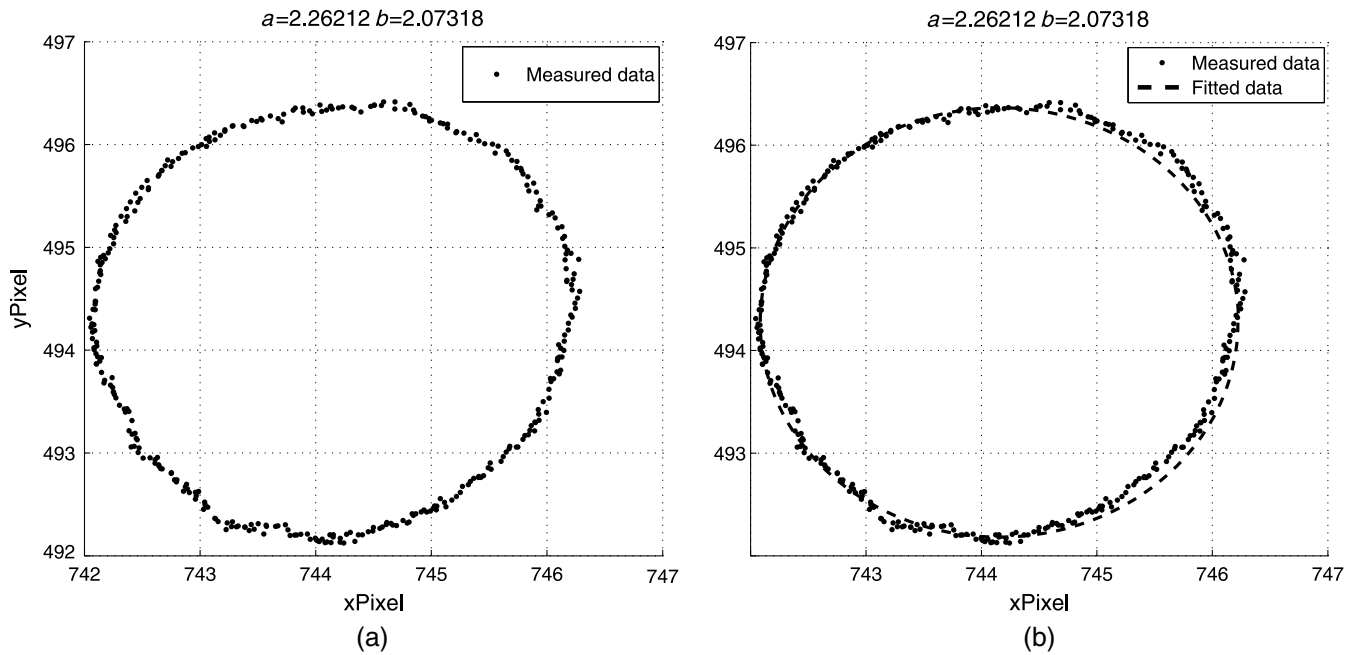


Fig. 8 Results of the calibration procedure: (a) Homogeneously distributed measured data. (b) Approximated ellipse.

other hand, the objective values are calculated with the middle diameter of the ellipse. Thus, it is not possible to converge to such low values as before. The calibration procedure is terminated after the 40th iteration, and the calculated optimal position is $p = (x, y, \alpha, \beta) = (3.945, -8.734, 0.719, 0.411)$. The results are shown in Fig. 8.

The residual motion of the optical image is about 2 pixels [Fig. 8(b)]. Due to the geometric conditions of the experimental setup, this corresponds to 1 mm. Focusing the homogeneous distribution of the measured data on the circumference in Fig. 8(a), the elimination of the miscalibration becomes clear. The uniform distribution excludes the presence of a movement with a small diameter generated by a miscalibration, already discussed in Fig. 7(d). Assessing

the operational capability, a further calibration procedure with a different starting position is initiated. Figure 9 shows the corresponding convergence process with the calculated optimal position $p = (16.147, -13.314, 0.521, -0.103)$.

It is obvious that the calibration algorithm converges to another local minimum. Referring to Sec. 3, this can be explained by the convertability of tiltings into shifts assuming small angles, illustrated in Fig. 10. Thus, the measurements validate the mathematical model.

In order to solve the problem, a two-step calibration would be possible. The calibration procedure explained above should be preceded by an identification of tiltings. For this purpose, the effect of perspective distortion could

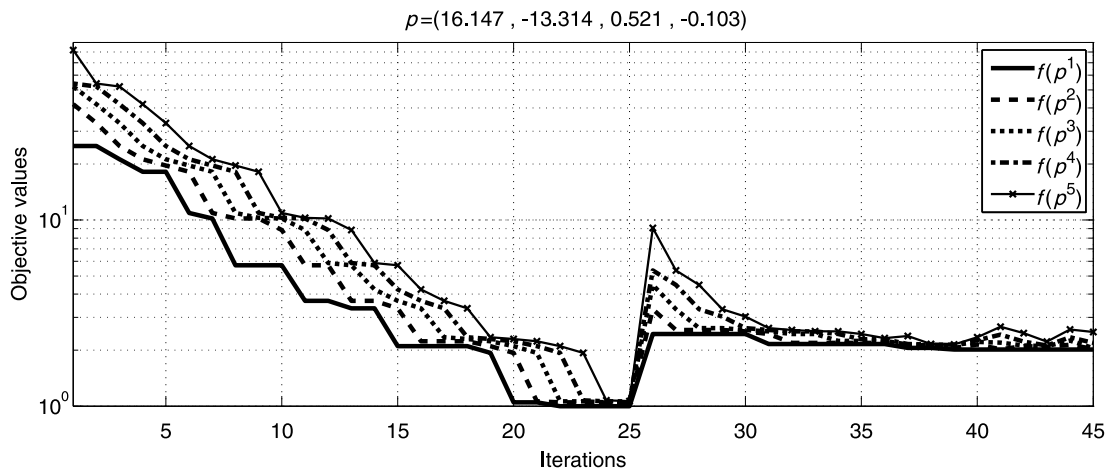


Fig. 9 Convergence of the objective values of a second calibration from a different starting position achieving a different position p .

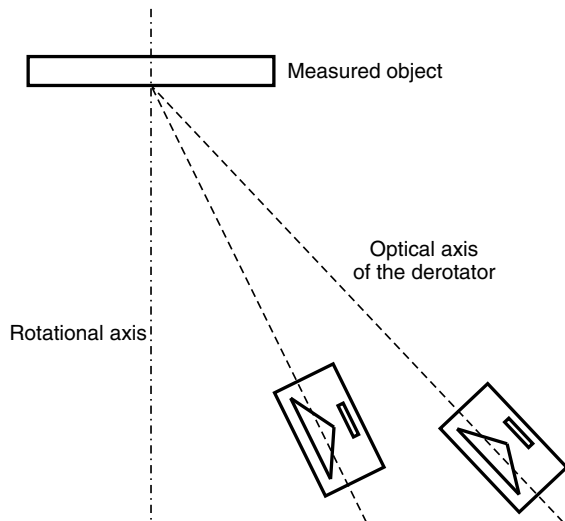


Fig. 10 Interchangeability of tiltings by shifts.

Table 1 Positions of the derotator from which the extent of a perspective distortion is determined.

x	20.000	18.000	16.000	...	-3.000
y	-8.734	-8.734	-8.734	...	-8.734
α	0.719	0.719	0.719	...	0.719
β	0.000	0.100	0.200	...	1.000

be useful. Regarding the results of the two calibration processes, it is questionable whether the perspective distortion is sensitive enough to tiltings in the range of ± 1 deg.

Within the scope of further experiments, the derotator stands still while the measured object shown in Fig. 4 rotates at a constant speed. This setup is used to identify the

elliptical path of the eccentric markers and to investigate the impact of different derotator positions. The positions are summarized in Table 1. An increase of the angle β is compensated by a shift in the negative x -direction. In each of these positions calculating the parameters a , b the elliptical path of the eccentric marker is approximated. The results are shown in Fig. 11.

Regardless of the angle β at each position, the same ellipse is identified. Effects of perspective distortion are not visible. This raises the question whether it is possible to identify small tilts with a two-dimensional object. Subsequent investigations should deal with the usability of three-dimensional (3-D) calibration phantoms. Mounted on the rotational axis of the measured object, they could provide more information about the location of the derotator compared with the measured object.

6 Conclusions

An optomechanical derotator is presented in this article, which makes it possible to apply optical measurement methods to rotating objects during operation. A stationary optical image can only be achieved if the optical axis of the derotator is coaxially aligned to the rotational axis of the measured object. For the calibration procedure, a mathematical model of the optical image is developed. Based on this model, a miscalibration is associated with the motion of the optical image. The aim of the calibration is to minimize this motion iteratively. Implementing industrial image processing algorithms, the motion is tracked with a high-speed camera. The path is approximated as a Limacon of Pascal using the particle swarm algorithm. One of the identified parameters represents the miscalibration. This is minimized by the Nelder–Mead algorithm, wherein the position of the derotator is changed with a hexapod. The results of the two calibration processes are compared. The Nelder–Mead algorithm converges to different local minima, because it is not possible to distinguish between tilts and shifts for small angles. The attempt to identify tiltings by a perspective distortion fails. As a possible solution to the problem, the use of 3-D calibration phantoms is suggested.

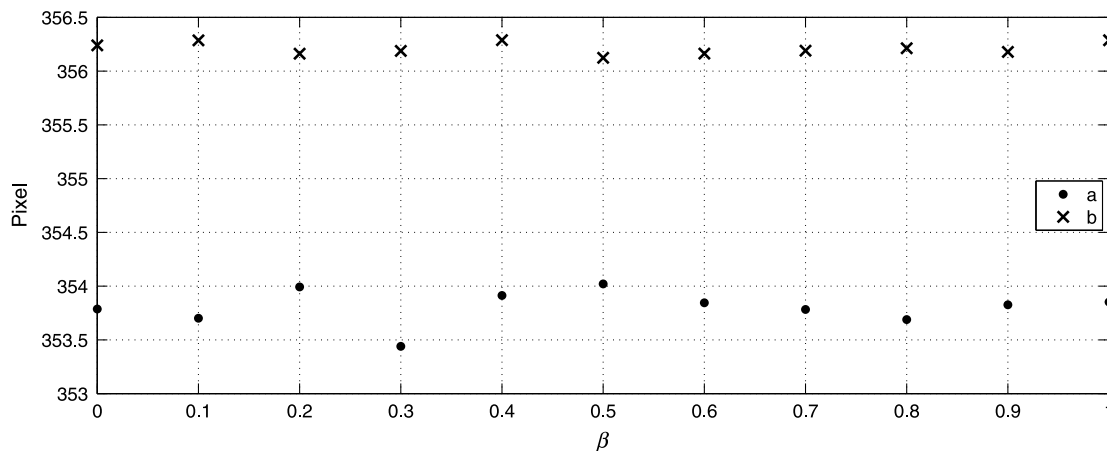


Fig. 11 Sensitivity of the parameters a , b approximating the elliptical path of the eccentric marker (averaged over three measurements).

References

1. S. Mirzaei et al., "Application of an optomechanical image derotator for measuring vibration and deformation of rotating objects," in *Proc. of the 4th International Conference on Optical Measurement Technique (Optimes)*, Antwerp, pp. 245–253 (2009).
2. E. Reithmeier, S. Mirzaei, and N. Kasyanenko, "Optical vibration and deviation measurement of rotating machine parts," *Optoelectron. Lett.* **4**(1), 45–48 (2008).
3. M. Rahlves et al., "In-plane and out-of-plane deformation and vibration measurement using an optomechanical image derotator," *Proc. SPIE* **7432**, 74320L (2009).
4. S. Mirzaei, "Entwicklung und Erprobung der Bildderotator-Messtechnik am Beispiel der Schlupfmessung von Waelzlagern," PhD Thesis, Leibniz Universitaet Hannover, Hannover (2011).
5. B. Rohloff et al., "Schwingungsanalyse von rotierenden objekten mit einem optomechanischen bildderotator," in *3. VDI-Fachtagung Schwingungsanalyse & Identifikation*, pp. 203–211, VDI Wissensforum GmbH, Düsseldorf (2013). ISBN 978-3-18-092191-4.
6. J. Miesner, "Beitrag zur kontinuierlichen interferometrischen Untersuchung der Eigenschwingformen rotierender Bauteile," PhD Thesis, Carl von Ossietzky Universitaet, Oldenburg (2004).
7. B. Rohloff et al., "Calibration of the optical axes of an image derotator using image processing and a 6-axes parallel kinematics," in *114. Jahrestagung der Deutschen Gesellschaft fuer angewandte Optik, Deutsche Gesellschaft für angewandte Optik e.V. (DGaO)*, Erlangen (2013).
8. B. Rohloff, "Calibration of an optomechanical image derotator with a 6-axes parallel kinematics using image processing algorithms," Scientific Reports 2011–2013 Institute of Measurement and Automatic Control, Vol. 4, pp. 45–50 (2013).
9. C. Demant, B. Streicher-Abel, and A. Springhoff, *Industrielle Bildverarbeitung*, Springer, Heidelberg (2011).
10. D. Schroeder, *Intelligente Verfahren—Identifikation und Regelung nichtlinearer Systeme*, Springer, Heidelberg (2010).
11. F. Jarre and J. Stoer, *Optimierung*, Springer, Berlin (2004).

Benjamin Rohloff received his diploma in industrial engineering from the Leibniz Universitaet Hannover in 2010. Since that time, he has been working as a research assistant at the Institute of Measurement and Automatic Control. His scientific work aims at the identification and control of nonlinear drive systems.

Christian Pape received his diploma in electrical engineering in 2004 and his PhD degree in mechanical engineering in 2011. His research interests are control engineering, robotics, and active noise reduction.

Eduard Reithmeier received his diploma in mechanical engineering in 1983, his diploma in mathematics in 1985, and the PhD degree from the Technische Universitaet Muenchen in 1989. He worked as a project engineer for BMW (Germany) and Mitsubishi Motors (Japan). After a postdoctoral research period at the University of California, Berkeley, he became technical divisional director at Bodenseewerk Geraetetechnik (Germany). Since 1995, he has led the Institute of Measurement and Automatic Control at the Leibniz Universitaet Hannover.